Altered Default Mode Network Is Associated With Cognitive Impairment in Cadasil as Revealed by Multimodal Neuroimaging

Panlong Li
Zhengzhou University of Light Industry
Qi Huang
Huashan Hospital Fudan University
Shiyu Ban
East China Normal University
Yuan Qiao
Shanghai 9th Peoples Hospital Affiliated to Shanghai Jiaotong University School of Medicine
Jing Wu
Shanghai 9th Peoples Hospital Affiliated to Shanghai Jiaotong University School of Medicine
Yu Zhai
Shanghai 9th Peoples Hospital Affiliated to Shanghai Jiaotong University School of Medicine
Xiaoxia Du
East China Normal University
Fengchun Hua
Shanghai University of TCM: Shanghai University of Traditional Chinese Medicine
Jingjing Su (jingjingsu2000@163.com)
Shanghai Jiao Tong University https://orcid.org/0000-0001-8527-0840

Research article

Keywords: CADASIL, default mode network, cognitive impairment, MRI, PET

Posted Date: July 6th, 2021

DOI: https://doi.org/10.21203/rs.3.rs-658208/v1

Version of Record: A version of this preprint was published at Frontiers in Neurology on December 6th, 2021. See the published version at https://doi.org/10.3389/fneur.2021.735033.

Abstract

Background: Cerebral autosomal dominant arteriopathy with subcortical infarcts and leukoencephalopathy (CADASIL) caused by mutations in NOTCH3 gene is a hereditary cerebral small vessel disease, manifesting with stroke, cognitive impairment and mood disturbances. Functional or structural changes in the default mode network (DMN), which plays important roles in cognitive and mental maintenance, have been found in a number of neurological and mental diseases. However, it is still unclear whether DMN is altered in CADASIL patients.

Methods: Multimodal imaging methods, including magnetic resonance imaging (MRI) and positron emission tomography (PET), were applied to evaluate the functional, structural and metabolic characteristics of DMN in 25 CADASIL patients and 42 healthy controls.

Results: Compared to controls, CADASIL patients had decreased nodal efficiency and degree centrality of the dorsal medial prefrontal cortex and hippocampal formation within DMN. Structural MRI and diffusion tensor imaging (DTI) showed decreased gray matter volume and fiber tracks presented in the bilateral hippocampal formation. Meanwhile, PET imaging showed decreased metabolism within the whole DMN in CADASIL. Furthermore, correlation analyses showed that these nodal characteristics, gray matter volume, and metabolic signals of DMN were related to cognitive scores in CADASIL.

Conclusions: Our results suggested that altered network characteristics of DMN may play important roles in cognitive deficits of CADASIL.

Background

Cerebral autosomal dominant arteriopathy with subcortical infarcts and leukoencephalopathy (CADASIL) is the most common hereditary cerebrovascular diseases [1]. It is caused by the pathogenic mutations in NOTCH3 gene on chromosome 19 and, therefore, shows familial inheritance. The typical clinical manifestations of CADASIL are migraine with aura, stroke, mood disturbances, and progressive cognitive impairments, including deficits in executive function, processing speed, attention, and memory [2].

Default mode network (DMN) is a notable network that shows greater activity during the resting state than when performing tasks. It was first addressed by Raichle in a positron emission tomography (PET) study in 2001 [3]. The component brain areas of DMN mainly include posterior cingulate cortex and precuneus (PCC/PCU), medial prefrontal cortex (MPFC), medial and inferior temporal lobes, and inferior parietal lobe (IPL), and play important roles in a great variety of cognitive domains, such as working memory, visuomotor, visual language, and mental imagery [4]. DMN has become a central research theme in neuropsychiatric disorders, including stroke, dementia, migraine, traumatic brain injury, depression, anxiety, and schizophrenia [5-10]. A number of magnetic resonance imaging (MRI) and PET studies have been widely used to explore DMN characteristics in these disorders [5-10]. However, as a focus of research into cognition, whether DMN is altered in CADASIL patients remains unclear.

Several studies have demonstrated the brain alterations in functional and structural imaging parameters in CADASIL patients. Our resting-state functional MRI (fMRI) studies showed that altered functional activity and connectivity in PCC/PCU and para-hippocampal cortex (PHC) were associated with cognitive impairment in CADASIL [11, 12]. Diffusion tensor imaging (DTI) studies have demonstrated widespread white matter lesions associated with cognitive deficits in CADASIL [13-15]. Moreover, a case study using diffusion tensor tractography indicated that neural tract injuries were mainly located in the frontal lobe in a patient with CADASIL [16]. Furthermore, a recent ^{18}F-2-fluoro-2-deoxy-d-glucose PET (^{18}F-FDG PET) study showed that decreased metabolism in limbic lobe, including the hippocampus and PHC, was positively associated with cognitive score in CADASIL patients [17]. Thus, based on the brain regions highlighted in these CADASIL studies, we assume that there may be alterations in DMN in these patients. This is because several regions involved in CADASIL belong to the hub nodes of DMN, and the DMN has a high degree of connectivity across the above involved regions, including the PCC/PCU, MPFC, hippocampus, and PHC [7, 18]. Therefore, it is necessary to explore whether changes in the DMN occur in CADASIL.

In the present study, we focused on multimodal imaging outcomes of DMN in CADASIL. Resting-state fMRI, T1-weighted MRI, DTI, and ^{18}F-FDG PET were employed to assess functional network properties, gray matter volume (GMV), structural connectivity, and metabolism in DMN, and the associations with cognitive deficits.

Methods

Participants

A total of 25 CADASIL patients from 14 families evaluated at Shanghai Ninth People's Hospital between May 2016 and January 2019 were recruited for this study. For all patients, the diagnosis was confirmed by identification of pathogenic mutations in the NOTCH3 gene [19]. All subjects underwent detailed standard neurological examinations. Subjects were excluded from the study if they had severe depression or anxiety according to evaluation by two trained neuropsychologists using the Hamilton Depression Scale (HAMD) and the Hamilton Anxiety Scale (HAMA) [20, 21]. Subjects were diagnosed with severe depression and anxiety based on HAMD and HAMA scores > 17 and > 14, respectively. Neurological deficits in all subjects were assessed using the National Institutes of Health Stroke Scale (NIHSS) and the modified Rankin scale (mRs). Cognitive scores in all subjects were recorded by the Montreal Cognitive Assessment (MoCA) and Mini-Mental State Examination (MMSE). Most of the patients underwent both MRI and PET/computed tomography (PET/CT), but four underwent only MRI and another four underwent only PET/CT.

Forty-two healthy subjects were recruited as a control group based on the following criteria: no history of stroke, headache, cognitive impairment or vascular disease risk factors; no family history of cerebrovascular diseases or vascular disease risk factors; not taking medications and no substance addiction, such as drugs, cigarettes, or alcohol. All of the healthy subjects had normal results on

neurological and general examinations. Twenty-one of the 42 controls underwent only MRI and the remaining 21 controls underwent only PET/CT. The sample size and demographic information of each group were listed in Table 1.

MRI acquisition

Subjects in the first control group and 21 CADASIL patients underwent MRI, including resting-state fMRI, structural MRI (T1-weighted, T2-weighted, and fluid-attenuated inversion recovery [FLAIR] imaging), and DTI on a 3.0 Tesla system (Trio Tim; Siemens Healthcare, Malvern, PA, USA) with a 12-channel head coil at East China Normal University. Soft earplugs and custom-fit foam were applied to reduce noise and movement artifacts. Resting-state fMRI was performed using a $T2^*$-weighted gradient-echo echo-planar imaging pulse sequence with the following parameters: repetition time/echo time (TR/TE) = 2000/30 ms; flip angle = 90°; field of view (FOV) = 220 × 220 mm^2; number of slices = 33; resolution = 3.44 × 3.44 × 4.38 mm^3; total volume = 210. During the fMRI scan, the subjects kept their eyes closed but did not fall asleep. The whole-brain anatomical volume was obtained using a high-resolution T1-weighted 3-dimensional magnetization-prepared rapid- acquisition gradient-echo pulse sequence with the following parameters: TR = 2530 ms; TE = 2.34 ms; flip angle = 7°; FOV = 256 × 256 mm^2; number of slices = 192; resolution = 1 × 1 × 1 mm^3. T2-weighted imaging was obtained using turbo spin echo dark fluid sequence with the following parameters: TR/TE = 5500/83 ms; FOV = 220 × 220 mm^2; number of slices = 33; resolution = 3.44 × 3.44 × 4.38 mm^3. The parameters of FLAIR imaging were: TR/TE = 9000/93 ms; FOV = 220 mm^2; number of slices = 33; resolution = 3.44 × 3.44 × 4.38 mm^3. DTI was performed using a single-shot, spin-echo planar imaging sequence acquired in contiguous axial planes with the following parameters: 64 noncollinear directions, diffusion weighting of b = 1000 s/m^2, an acquisition without diffusion weighting of b = 0; TR/TE = 8900/86 ms; FOV = 256 × 256 mm^2, covered the whole brain; 70 contiguous slices; resolution = 2 × 2 × 2 mm^3.

PET acquisition

^{18}F-FDG PET data were acquired using a Siemens Biograph Truepoint HD 64 PET/CT at the PET Center of Huashan Hospital, Fudan University. ^{18}F-FDG was synthesized and radiolabeled at the PET Center according to the manufacturer's protocol under inspection of the Chinese Food and Drug Administration. Before ^{18}F-FDG injection, subjects were asked to avoid strenuous physical activity and fast for about 6 hours to maintain blood glucose level < 8.0 mmol/L. After receiving injection of ^{18}F-FDG at a dose of 5.55 MBq/kg [0.15 mCi/kg], subjects rested in a dimly lit room for 50 minutes. Before PET acquisition, a low-dose CT scan was performed for attenuation correction, and then 10-min PET images were reconstructed using a filtered back-projection algorithm. The matrix size of the reconstructed images was 168 × 168 × 148 with resolution of 2.04 × 2.04 × 1.5 mm^3.

Data processing

Prior to preprocessing, all the raw DICOM data were converted to the Neuroimaging Informatics Technology Initiative format (NII) using MRICRON software (http://people.cas.sc.edu/rorden/mricron/install.html) and the quality of the images was checked visually.

fMRI data processing

The resting-state fMRI data were preprocessed using Data Processing Assistant for Resting-State fMRI (DPARSF; http://www.restfmri.net) [22, 23]. Data were preprocessed starting with removal of the first 10 volumes to ameliorate possible effects of scanner instability and the adaptation of subjects to the environment. Then, slice time correction was applied to reduce the effects of within-scan acquisition time differences between slices. To correct the effects of head motion, the fMRI images of each subject were realigned and registered. All subjects had head motions < 1.5° of rotation or 0.5 mm of mean frame wise displacement [24]. The fMRI images were then normalized into the Montreal Neurological Institute (MNI) space using the EPI template and smoothed by a full-width at half-maximum (FWHM) 8 mm Gaussian kernel. Following spatial smoothing, linear detrend was performed to remove noise due to long-term physiological shifts, movement-related noise remaining after realignment, and instrumental instability. To reduce further the effects of noise, the fMRI images were filtered with a temporal band-pass filter (0.01–0.08 Hz). Finally, the six head motion parameters, global mean signal, white matter signal, and cerebrospinal fluid signal were regressed out as nuisance covariates to remove these unwanted signals.

With reference to previous studies [18, 25, 26], 11 separate regions comprising the left DMN and 11 mirrored regions comprising the right DMN were defined as regions of interest (ROIs). The 11 ROIs were spheres of radius 8 mm in the dorsal MPFC (dMPFC), anterior MPFC (aMPFC), ventral MPFC (vMPFC), posterior IPL (pIPL), temporal parietal junction (TPJ), lateral temporal cortex (LTC), temporal pole (TempP), PCC, retrosplenial cortex (RSC), PHC, and hippocampal formation (HF) (See Supplemental Table 1 and Supplemental Figure 1 for coordinates and spatial positions). Average fMRI time-series were calculated across every voxel in each ROI. The absolute value of Fisher's z-transformed Pearson's correlation coefficient between each pair of time-series was defined as the functional connectivity (FC) strength.

Graph analysis of the pairwise (11 × 11) correlation matrixes was performed using GRETNA (v2.0.0; https://www.nitrc.org/projects/gretna/) [27]. Global and nodal network properties, including nodal degree centrality, nodal shortest path length, nodal clustering coefficient, nodal efficiency, nodal local efficiency, betweenness centrality, global efficiency, assortativity coefficient, and small-worldness, were calculated to delineate the integrative and local topological architecture of the DMN, respectively. Their definitions and calculations of the nodal and global network properties were summarized in Supplemental Table 2.

T1-weighted data processing

The T1-weighted MRI data were preprocessed using the Computational Anatomy Toolbox (CAT12; http://dbm.neuro.uni-jena.de/cat12) implemented in statistical parametric mapping software (SPM12; htttp://www.fil.ion.ucl.ac.uk/spm/). First, all T1-weighted MRI data were normalized into the MNI space using the Diffeomorphic Anatomic Registration Through Exponentiated Lie algebra algorithm (DARTEL). The bias field inhomogeneities were corrected to remove non-uniform intensities. Normalized images were then segmented into gray matter, white matter, and cerebrospinal fluid components. The total intracranial volume (TIV) of each participant was evaluated to correct for the effects of differences in brain size. The internal gray matter threshold was set to 0.2 to exclude artifacts on the gray–white matter border. Thereafter, all preprocessed scans were smoothed with the FWHM 6 mm Gaussian kernel. Finally, average GMV was calculated across every voxel in each ROI.

DTI data processing

The raw DTI data were preprocessed using FMRIB Software Library (FSL; http://www.fmrib.ox.ac.uk/fsl/index.html). First, eddy current correction was performed to correct for head motion artifacts and eddy current distortions. Then, the brain of each subject was extracted using the FSL Brain Extraction Tool (BET). Tensor reconstruction and fiber tracking were applied by Diffusion Toolkit TrackVis (https://www.nitrc.org/projects/trackvis). The Fiber Association Continuous Tracking (FACT) algorithm in Diffusion Toolkit was applied to obtain the whole-brain fiber tracts. The main parameters in fiber tractography were as follows: maximum turning angle threshold at 35°; minimum fractional anisotropy (FA) threshold of 0.2. Then, SPM12 was applied to bring all the individual tracts into the MNI space by nonlinear transformation methods. In the normalization step, tracts were spatially normalized by: coregistering T1-weighted MRI to the corresponding FA image; calculating the deformation field of the individual coregistered T1-weighted image space to the MNI space; and applying the deformation field to tracts and bringing them into the MNI space. Thereafter, TrackVis was used to record the number of tracts (NT) passing through each ROI.

PET data processing

First, PET images of each subject were processed using SPM12 software with spatial normalization and smoothing. The PET template in SPM12 was used in the spatial normalization step. The FWHM 8 mm Gaussian kernel was applied in the smoothing step. The average glucose metabolism was then calculated across every voxel in each ROI.

Statistical analysis

Statistical analysis was performed using IBM SPSS Statistics for Windows (SPSS, Chicago, IL, USA). The Chi-square tests and permutation tests (permutation times = 10,000) were used to compare demographic,

clinical, and imaging characteristics between the CADASIL and control groups, as appropriate. Further, the two-sample *t* test was applied for voxel-wise metabolism comparisons between the CADASIL and corresponding control groups using SPM12 software. Subsequently, partial correlations were established to estimate the relations between the cognitive deficits and the imaging characteristics showing significant between-group differences. Age, sex, and education levels were entered as covariates in partial correlation analysis. Benjamini-Hochberg false discovery rate (FDR) correction was further used to avoid type-I errors in the multiple comparisons and correlations. The results of two-sample comparisons and partial correlations were regarded significant at $p < 0.05$ (two-tailed) with FDR correction.

Results

Demographic and clinical data

Table 1 showed comparisons of the demographic and clinical data of the CADASIL and healthy control groups. There were significant differences between the two groups in terms of neurological deficits and cognitive scores, but no differences in sex, age, education levels, or depression and anxiety symptom scores.

Table 1. Demographic information of CADASIL and controls

	CADASIL (n = 25)		Controls (n = 42)		*p* values	
	MRI (n = 21) PET (n = 21)		MRI (n = 21) PET (n = 21)		*p*1	*p*2
Male/female	13/8	14/7	13/8	14/7	1	1
Age (years), mean ± SD	48.4 ± 14.2	46.3 ± 14.0	48.7 ± 14.3	45.8 ± 12.1	0.9	0.9
Education (years), mean ± SD	8.7 ± 3.5	8.9 ± 3.3	9.1 ± 3.2	9.3 ± 3.0	0.8	0.8
Family history, *n* (%)	20 (95.2)	21 (100)	-	-	-	-
Migraine, *n* (%)	3 (14.3)	3 (14.3)	-	-	-	-
Migraine with aura, *n* (%)	2 (9.5)	2 (9.5)	-	-	-	-
Migraine without aura, *n* (%)	1 (4.8)	1 (4.8)	-	-	-	-
Previous stroke or TIA (times), median ± IQR	2 ± 3	2 ± 3	-	-	-	-
HAMD, median ± IQR	4 ± 6	4 ± 5	3 ± 4	3 ± 3	0.3	0.3
HAMA, median ± IQR	3 ± 1	3 ± 1	3 ± 1	3 ± 2	0.7	0.7
NIHSS, median ± IQR	0 ± 1	0 ± 1	0 ± 0	0 ± 0	0.01	0.006
mRs, median ± IQR	1 ± 2	1 ± 2	0 ± 0	0 ± 0	0.001	0.001
MoCA, median ± IQR	21 ± 15	20 ± 11	26 ± 3	27 ± 1	0.000	0.000
MMSE, median ± IQR	24 ± 12	24 ± 11	28 ± 1	28 ± 2	0.001	0.002

Note: SD and IQR represent standard deviation and interquartile range, respectively. P1 represents *p* values of the comparisons between patients and controls in MRI group, and *p*2 represents *p* values of the comparisons between patients and controls in PET group. CADASIL, cerebral autosomal dominant arteriopathy with subcortical infarcts and leukoencephalopathy; MRI, magnetic resonance imaging; PET, positron emission tomography; TIA, transient ischemic attack; HAMD, Hamilton Depression Scale; HAMA, Hamilton Anxiety Scale; NIHSS, National Institute of Health Stroke Scale; mRS, modified Rankin scale; MoCA, Montreal Cognitive Assessment; MMSE, Mini-Mental State Examination.

Network analysis of DMN

Compared to the healthy control group, the CADASIL group had decreased FC between the HF and the MPFC (aMPFC, dMPFC, and vMPFC), as well as increased FC between the TPJ and PHC within the left DMN (Figure 1A and Supplemental Figure 2). Further network analysis showed that the nodal characteristics of the left dMPFC and HF, including nodal efficiency and degree centrality, were significantly different between the CADASIL and healthy control groups (Figure 2A). The integrative topological architecture of the left DMN was not significantly different between the two groups.

In the right DMN, the CADASIL group showed decreased FC between the HF and the aMPFC as well as the dMPFC, and increased FC between the TPJ and RSC in comparison to the healthy control group (Figure 1B and Supplemental Figure 2). There were no significant differences in the global or local topological architecture of the right DMN between the two groups.

GMV analysis of DMN

There was no significant difference in TIV between the CADASIL group and the healthy control group. Compared to the healthy control group, the CADASIL patients had decreased GMV in the left PHC (0.58 ± 0.10 vs. 0.66 ± 0.12, respectively, $p = 0.02$) and bilateral HF (left: 0.38 ± 0.04 vs. 0.41 ± 0.05, respectively, $p = 0.035$; right: 0.40 ± 0.05 vs. 0.44 ± 0.06, respectively, $p = 0.04$) (Figure 3A).

Fiber tracks analysis of DMN

Compared to the healthy control group, the CADASIL patients had reduced NT in the bilateral HF (left:198.86 ± 85.86 vs. 263.33 ± 64.18, respectively, $p = 0.008$; right: 208.05 ± 72.68 vs. 290.24 ± 84.01, respectively, $p = 0.001$) (Figure 4). There was no significant increase in tracks between the CADASIL and healthy control groups.

Metabolism analysis of DMN

Compared to the healthy control group, the CADASIL patients had decreased glucose metabolism across the ROIs ($p < 0.00001$) (Figure 5A). There was a significant decrease in global metabolism across the whole brain ($p < 0.00001$) (Figure 5A). There was no significant difference in regional metabolism between the two groups.

Correlation analysis

In fMRI, the nodal efficiency and degree centrality in the bilateral HF were positively correlated with MoCA and MMSE scores in the CADASIL patients ($p < 0.05$) (Figure 2B). Similar correlations between the GMV of the bilateral HF and left PHC, and cognitive scores were also detected in the CADASIL group (Figure 3B). There was no significant correlation between number of tracks and cognitive scores. The levels of

metabolism in most ROIs with decreased glucose metabolism were positively correlated with the cognitive scores in the CADASIL group ($p < 0.01$) (Figure 5B and Supplemental Table 3).

Discussion

The present study was performed to investigate whether the DMN network was altered in CADASIL patients. We integrated the results of multimodal imaging methods, including fMRI, T1-weighted MRI, DTI, and PET, to investigate the changes in functional network properties, GMV, fiber tracks, and glucose metabolism within the DMN in patients with CADASIL. Consistent with our initial hypothesis, the characteristics of DMN represented by these images in the CADASIL group were significantly different compared to those in the healthy control group. Correlation analysis showed that these characteristics were associated with cognitive deficits in the CADASIL group.

In FC analysis, weakened interactions between the HF and MPFC (aMPFC and dMPFC) were detected in both the left and right DMN in patients with CADASIL. Further graph theory analysis of the FC matrixes showed that the changed FC resulted in decreased nodal efficiency and degree centrality of HF and dMPFC in the CADASIL group. These observations indicated that HF and dMPFC within the DMN in the CADASIL patients has poor capacity for information propagation, and reduced functional interactions with other regions within the network. Indeed, the HF plays a central node in memory function [28-30] and the dMPFC plays a key role in cognitive performance, including decision making, reward processing, mentalizing, memory, and conceptual processing [9, 30, 31]. In addition, functional interactions between the HF and MPFC have been demonstrated to form an important neural circuit for spatial working memory [32-34]. Furthermore, functional alterations in the HF or MPFC have been shown to be associated with cognitive deficits in other diseases [35-39]. Therefore, our fMRI results demonstrated that the changed FC strength as a particular locus of dysfunction affected the nodal properties of the DMN, which may contribute to cognitive deficits in CADASIL patients.

To examine structural changes within the DMN in CADASIL, differences between the two groups in GMV and NT of the ROIs were examined. Analyses of both the GMV and NT showed that CADASIL patients had decreased GMV and NT in the ROI of HF. Further, decreased GMV was found in the left PHC and the bilateral HF in the CADASIL group. Both the PHC and HF are key regions for memory-related cognition [30, 40, 41]. In addition, decreased GMV as well as changed FA in the two regions have been reported to be associated with cognitive deficits [13, 42-44]. The significant associations between the GMV of HF and cognitive scores were consistent with the results of a previous MRI study in a large cohort [45]. In fact, the HF belongs to the medial temporal subsystem of the DMN, which, through its interactions with the MPFC, plays a role in a wide range of associative or constructive aspects of mental simulation [9]. Indeed, decreased interactions between the MPFC and medial temporal lobe including the hippocampus in resting-state fMRI data, and decreased GMV in the two regions, have been suggested to be associated with cognitive deficits, including working memory, social and emotional processing, and executive function deficits [38, 39, 42-44, 46, 47]. The two regions have been suggested to play hub roles in DMN, which is a hub network for advanced cognition [18, 25]. Cognitive performance relies on the coordination

and collaboration of the activation and deactivation response; if one component fails, the whole system is jeopardized [48, 49]. Therefore, the overlap between the results of fMRI and structural MRI indicates that changes of HF within the DMN may play important roles in the cognitive deficits seen in CADASIL patients.

In marked contrast to the local variation in MRI results, ^{18}F-FDG PET showed that glucose metabolism of each ROI within the whole DMN, and even the whole brain, was decreased in the CADASIL group. Although there have been few PET studies in CADASIL, two independent PET studies reported hypometabolism across the whole brain in the resting state in CADASIL patients [50, 51], which was consistent with our findings. Furthermore, similar to the results of MRI, metabolism was positively correlated with the cognitive scores in the CADASIL group. These correlations between characteristics of DMN revealed by different imaging modalities and cognitive scores suggested that interior relations may underlie the functional and structural changes within the DMN in CADASIL patients. However, regional functional or structural disconnection can affect metabolism in other regions, and vice versa. Further longitudinal multimodal imaging studies are required to determine the underlying mechanisms.

This study had some limitations, as only resting-state fMRI or PET data were collected, and it is therefore unclear whether there are altered patterns of DMN activity or connectivity during task performance in CADASIL, which have been demonstrated in other disorders or with aging [52-55].

Conclusions

In conclusion, altered functional and structural properties of the DMN were found in CADASIL patients by multimodal imaging. These cognition-associated changes of HF within the DMN may play important roles in cognitive deficits in CADASIL.

Abbreviations

CADASIL: cerebral autosomal dominant arteriopathy with subcortical infarcts and leukoencephalopathy; DMN: default mode network; MRI: magnetic resonance imaging; PET: positron emission tomography; DTI: diffusion tensor imaging; GMV: gray matter volume; MoCA: Montreal Cognitive Assessment; MMSE: Mini-Mental State Examination; MPFC: medial prefrontal cortex; HF: hippocampal formation; PHC: para-hippocampal cortex.

Declarations

• Ethics approval and consent to participate

The study protocol was approved by the Independent Ethics Committee of Shanghai Ninth People's Hospital, Huashan Hospital and East China Normal University. All participants were fully informed of the study procedures and provided written informed consents.

• **Consent for publication**

Not applicable.

• **Availability of data and materials**

The datasets used and analysed during the current study are available from the corresponding author on reasonable request.

• **Competing interests**

The authors declare that they have no conflict of interest.

• **Funding**

This research was supported by grants from the National Natural Science Foundation of China (82071282 to J.J. Su), the Rare Disease Registration Platform of Shanghai Ninth People's Hospital, Shanghai Jiao Tong University School of Medicine (JYHJB08 to J.J. Su), and the Horizontal Research Project from Shanghai Ninth People's Hospital (JYHX2021001 to J.J. Su).

• **Authors' contributions**

Study conception and design: Jingjing Su, Fengchun Hua, Xiaoxia Du; acquisition of data: Panlong Li, Qi Huang, Jing Wu, Yuan Qiao, Yu Zhai; analysis and interpretation of data: Panlong Li, Shiyu Ban; drafting the article: all authors; final approval of the version to be published: all authors.

• **Acknowledgements**

We would like to gratefully thank the patients and healthy volunteers taking part in this study.

References

1. Di Donato I, Bianchi S, De Stefano N, Dichgans M, Dotti MT, Duering M et al (2017) Cerebral Autosomal Dominant Arteriopathy with Subcortical Infarcts and Leukoencephalopathy (CADASIL) as a model of small vessel disease: update on clinical, diagnostic, and management aspects. BMC Med 15(1):41
2. Davous P (1998) CADASIL: a review with proposed diagnostic criteria. Eur J Neurol 5:219–233
3. Raichle ME, MacLeod AM, Snyder AZ, Power WJ, Gusnard DA, Shulman GL (2001) A default mode of brain function. Proc Natl Acad Sci USA 98(2):676–682
4. Hu ML, Zong XF, Mann JJ, Zheng JJ, Liao YH, Li ZC et al (2017) A Review of the Functional and Anatomical Default Mode Network in Schizophrenia. Neurosci Bull 33(1):73–84
5. Zong X, Hu M, Pantazatos SP, Mann JJ, Wang G, Liao Y et al (2019) A Dissociation in Effects of Risperidone Monotherapy on Functional and Anatomical Connectivity Within the Default Mode

Network. Schizophr Bull 45(6):1309–1318

6. Rodriguez-Cano E, Alonso-Lana S, Sarro S, Fernandez-Corcuera P, Goikolea JM, Vieta E et al (2017) Differential failure to deactivate the default mode network in unipolar and bipolar depression. Bipolar Disord 19(5):386–395
7. Menon V (2011) Large-scale brain networks and psychopathology: a unifying triple network model. Trends in Cognitive Sciences 15(10):483–506
8. Guo X, Duan X, Suckling J, Chen H, Liao W, Cui Q et al (2019) Partially impaired functional connectivity states between right anterior insula and default mode network in autism spectrum disorder. Hum Brain Mapp 40(4):1264–1275
9. Andrews-Hanna JR, Smallwood J, Spreng RN (2014) The default network and self-generated thought: component processes, dynamic control, and clinical relevance. Ann N Y Acad Sci 1316(1):29–52
10. Messina R, Filippi M, Goadsby PJ (2018) Recent advances in headache neuroimaging. Curr Opin Neurol 31(4):379–385
11. Su J, Ban S, Wang M, Hua F, Wang L, Cheng X et al (2019) Reduced resting-state brain functional network connectivity and poor regional homogeneity in patients with CADASIL. J Headache Pain 20(1):103
12. Su J, Wang M, Ban S, Wang L, Cheng X, Hua F et al (2019) Relationship between changes in resting-state spontaneous brain activity and cognitive impairment in patients with CADASIL. J Headache Pain 20(1):36
13. Ban S, Wang H, Wang M, Xu S, Qin Z, Su J et al (2019) Diffuse Tract Damage in CADASIL Is Correlated with Global Cognitive Impairment. Eur Neurol 81(5–6):294–301
14. Viswanathan A, Godin O, Jouvent E, O'Sullivan M, Gschwendtner A, Peters N et al (2010) Impact of MRI markers in subcortical vascular dementia: A multi-modal analysis in CADASIL. Neurobiol Aging 31(9):1629–1636
15. Molko N, Pappata S, Mangin JF, Poupon F, LeBihan D, Bousser MG et al (2002) Monitoring disease progression in CADASIL with diffusion magnetic resonance imaging: a study with whole brain histogram analysis. Stroke 33(12):2902–2908
16. Jang SH, Seo YS (2015) Injuries of neural tracts in a patient with CADASIL: a diffusion tensor imaging study. BMC Neurol 15:176
17. Su J, Huang Q, Ren S, Xie F, Zhai Y, Guan Y et al (2019) Altered Brain Glucose Metabolism Assessed by (18)F-FDG PET Imaging Is Associated with the Cognitive Impairment of CADASIL. Neuroscience 417:35–44
18. Andrews-Hanna JR, Reidler JS, Sepulcre J, Poulin R, Buckner RL (2010) Functional-anatomic fractionation of the brain's default network. Neuron 65(4):550–562
19. Joutel A, Corpechot C, Ducros A, Vahedi K, Chabriat H, Mouton P et al (1996) Nothc3 mutations in CADASIL, a hereditary adult-onset condition causing stroke and dementia. Nature 383(24):707–710

20. Zimmerman M, Thompson JS, Diehl JM, Balling C, Kiefer R (2020) Is the DSM-5 Anxious Distress Specifier Interview a valid measure of anxiety in patients with generalized anxiety disorder: A comparison to the Hamilton Anxiety Scale. Psychiatry Res 286:112859
21. Mozen-Zadeh E, Bayanati S, Ziafat K, Rezaei F, Mesgarpour B, Akhondzadeh S (2020) Vortioxetine as adjunctive therapy to risperidone for treatment of patients with chronic schizophrenia: A randomised, double-blind, placebo-controlled clinical trial. Journal of Psychopharm 34(5):506–513
22. Chao-Gan Y, Yu-Feng Z (2010) DPARSF: A MATLAB Toolbox for "Pipeline" Data Analysis of Resting-State fMRI. Front Syst Neurosci 4:13
23. Yan CG, Wang XD, Zuo XN, Zang YF (2016) DPABI: Data Processing & Analysis for (Resting-State). Brain Imaging Neuroinformatics 14(3):339–351
24. Power JD, Barnes KA, Snyder AZ, Schlaggar BL, Petersen SE (2012) Spurious but systematic correlations in functional connectivity MRI networks arise from subject motion. Neuroimage 59(3):2142–2154
25. Buckner RL, Andrews-Hanna JR, Schacter DL (2008) The brain's default network: anatomy, function, and relevance to disease. Ann N Y Acad Sci 1124:1–38
26. Buckner RL, Sepulcre J, Talukdar T, Krienen FM, Liu H, Hedden T et al (2009) Cortical hubs revealed by intrinsic functional connectivity: mapping, assessment of stability, and relation to Alzheimer's disease. J Neurosci 29(6):1860–1873
27. Wang J, Wang X, Xia M, Liao X, Evans A, He Y (2015) GRETNA: a graph theoretical network analysis toolbox for imaging connectomics. Front Hum Neurosci 9:386
28. Eichenbaum H (2015) Does the hippocampus preplay memories? Nat Neurosci 18(12):1701–1702
29. Bird CM (2017) The role of the hippocampus in recognition memory. Cortex 93:155–165
30. Hainmueller T, Bartos M (2018) Parallel emergence of stable and dynamic memory engrams in the hippocampus. Nature 558(7709):292–296
31. Lv C, Wang Q, Chen C, Xue G, He Q, Activation patterns of the dorsal medial prefrontal cortex and frontal pole predict individual differences in decision impulsivity. Brain Imaging Behav, 2020
32. Hyman, Working memory performance correlates with prefrontal-hippocampal theta interactions but not with prefrontal neuron firing rates. Frontiers in Integrative Neuroscience, 2010
33. Benchenane K, Peyrache A, Khamassi M, Tierney PL, Gioanni Y, Battaglia FP et al (2010) Coherent theta oscillations and reorganization of spike timing in the hippocampal- prefrontal network upon learning. Neuron 66(6):921–936
34. Wirt RA, Hyman JM, Integrating Spatial Working Memory and Remote Memory: Interactions between the Medial Prefrontal Cortex and Hippocampus. Brain Sci, 2017. 7(4)
35. Moran JM, Jolly E, Mitchell JP (2012) Social-Cognitive Deficits in Normal Aging. J Neurosci 32(16):5553–5561
36. Pasquini L, Scherr M, Tahmasian M, Meng C, Myers NE, Ortner M et al (2015) Link between hippocampus' raised local and eased global intrinsic connectivity in AD. Alzheimer's Dement

11(5):475–484

37. Zhu L, Shu H, Liu D, Guo Q, Wang Z, Zhang Z, Apolipoprotein E (2018) epsilon4 Specifically Modulates the Hippocampus Functional Connectivity Network in Patients With Amnestic Mild Cognitive Impairment. Front Aging Neurosci 10:289
38. Tao J, Liu J, Chen X, Xia R, Li M, Huang M et al (2019) Mind-body exercise improves cognitive function and modulates the function and structure of the hippocampus and anterior cingulate cortex in patients with mild cognitive impairment. Neuroimage Clin 23:101834
39. Liang L, Zhao L, Wei Y, Mai W, Duan G, Su J et al (2020) Structural and Functional Hippocampal Changes in Subjective Cognitive Decline From the Community. Front Aging Neurosci 12:64
40. Brown TI, Stern CE (2014) Contributions of medial temporal lobe and striatal memory systems to learning and retrieving overlapping spatial memories. Cereb Cortex 24(7):1906–1922
41. Eichenbaum H (2017) On the Integration of Space, Time, and Memory. Neuron 95(5):1007–1018
42. Konishi K, McKenzie S, Etchamendy N, Roy S, Bohbot VD (2017) Hippocampus-dependent spatial learning is associated with higher global cognition among healthy older adults. Neuropsychologia 106:310–321
43. Jirsaraie RJ, Sheffield JM, Barch DM (2018) Neural correlates of global and specific cognitive deficits in schizophrenia. Schizophr Res 201:237–242
44. Chen B, Fan GG, Liu H, Wang S (2015) Changes in anatomical and functional connectivity of Parkinson's disease patients according to cognitive status. Eur J Radiol 84(7):1318–1324
45. O'Sullivan M, Ngo E, Viswanathan A, Jouvent E, Gschwendtner A, Saemann PG et al (2009) Hippocampal volume is an independent predictor of cognitive performance in CADASIL. Neurobiol Aging 30(6):890–897
46. Wang L, Zang Y, He Y, Liang M, Zhang X, Tian L et al (2006) Changes in hippocampal connectivity in the early stages of Alzheimer's disease: evidence from resting state fMRI. Neuroimage 31(2):496–504
47. Kennedy DP, Courchesne E, The intrinsic functional organization of the brain is altered in autism. Neuroimage, 2008. 39(4): p. 1877–85
48. Broyd SJ, Demanuele C, Debener S, Helps SK, James CJ, Sonuga-Barke EJ (2009) Default-mode brain dysfunction in mental disorders: a systematic review. Neurosci Biobehav Rev 33(3):279–296
49. Wermke M, Sorg C, Wohlschlager AM, Drzezga A (2008) A new integrative model of cerebral activation, deactivation and default mode function in Alzheimer's disease. Eur J Nucl Med Mol Imaging 35(Suppl 1):S12–S24
50. Tuominen S, Miao Q, Kurki T, Tuisku S, Pöyhönen M, Kalimo H et al (2004) Positron Emission Tomography Examination of Cerebral Blood Flow and Glucose Metabolism in Young CADASIL Patients. Stroke 35(5):1063–1067
51. Tatsch K, Koch W, Linke R, Poepperl G, Peters N, Holtmannspoetter M et al (2003) Cortical Hypometabolism and Crossed Cerebellar Diaschisis Suggest Subcortically Induced Disconnection in

CADASIL: An ^{18}F-FDG PET Study. The Journal of Nuclear Medicine 44(6):862–869

52. Andrews-Hanna JR, Snyder AZ, Vincent JL, Lustig C, Head D, Raichle ME et al (2007) Disruption of large-scale brain systems in advanced aging. Neuron 56(5):924–935
53. Kennedy DP, Redcay E, Courchesne E, Falling to deactivate: Resting functional abnormalities in autism. Proceedings of the National Academy of Sciences (2006) **103**(21): p. 8275–8280
54. Li LM, Violante IR, Leech R, Ross E, Hampshire A, Opitz A et al (2018) Brain state and polarity dependent modulation of brain networks by transcranial direct current stimulation. Hum Brain Mapp 40(3):904–915
55. Hughes C, Faskowitz J, Cassidy BS, Sporns O, Krendl AC (2020) Aging relates to a disproportionately weaker functional architecture of brain networks during rest and task states. Neuroimage 209:116521

Figures

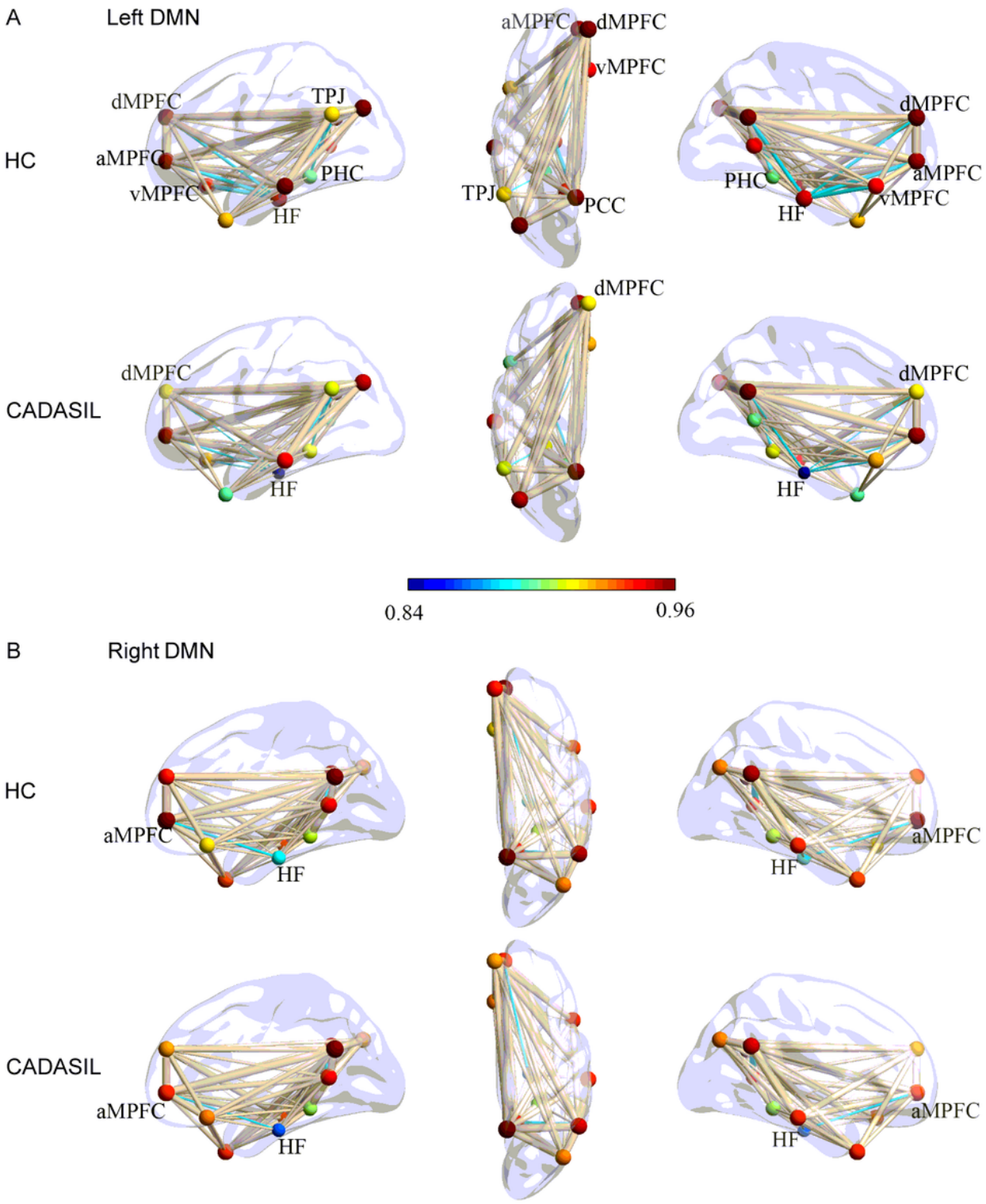

Figure 1

Topological properties of DMN in CADASIL and control groups in the left (A) and right (B) hemisphere. The color bar corresponded to nodal color, representing the mean nodal efficiency in the corresponding group. Nodal size represented the mean degree centrality in the corresponding group. The thickness of edges reflected the strength of FC between regions. FC showing significant differences between the two groups was indicated in cyan ($p < 0.05$). DMN, default mode network; CADASIL, cerebral autosomal

dominant arteriopathy with subcortical infarcts and leukoencephalopathy; FC, functional connectivity; HC, healthy control; aMPFC, anterior medial prefrontal cortex; dMPFC, dorsal medial prefrontal cortex; vMPFC, ventral medial prefrontal cortex; HF, hippocampal formation; PCC, posterior cingulate cortex; PHC, parahippocampal cortex; TPJ, temporal parietal junction.

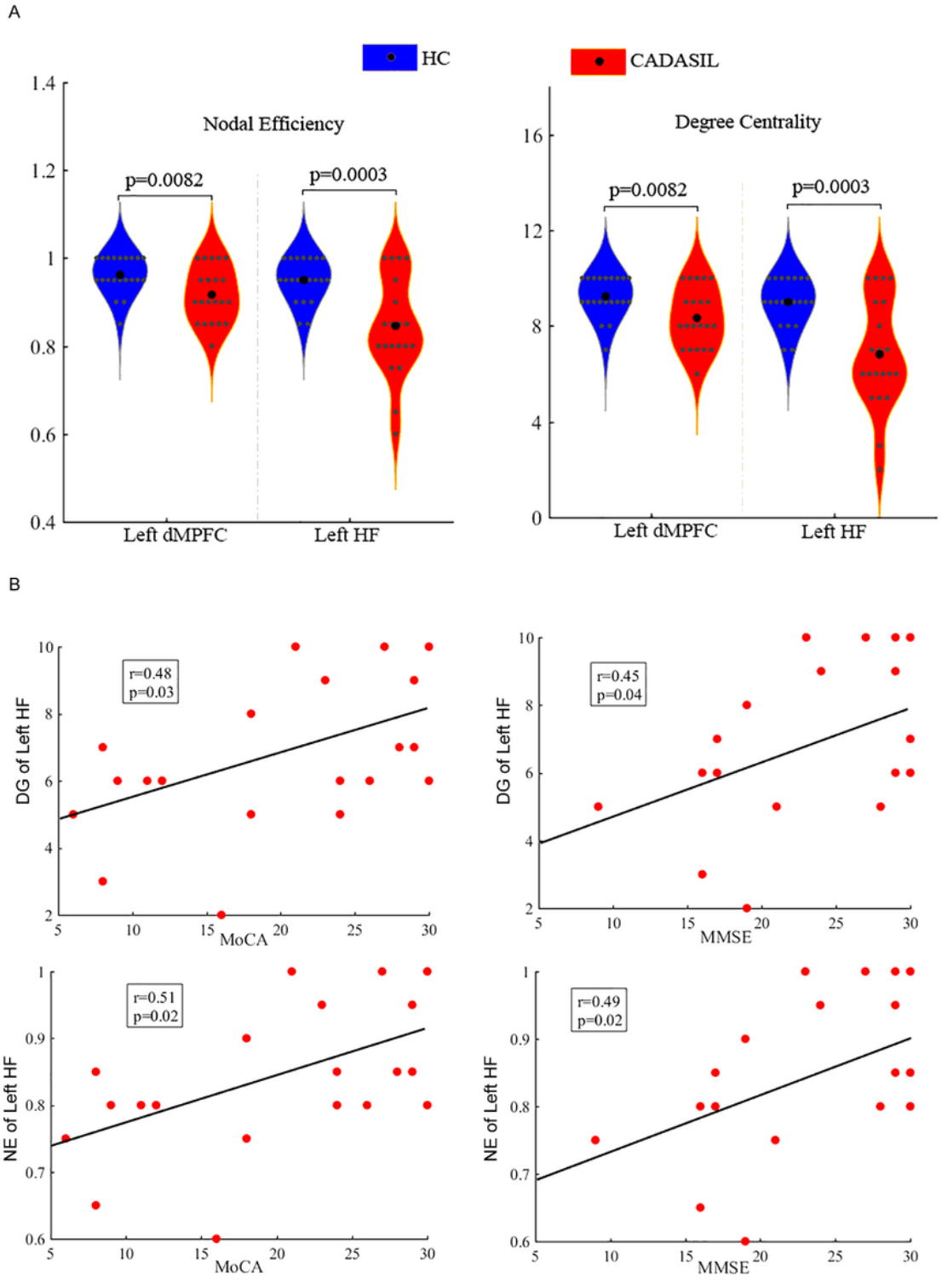

Figure 2

Differences between CADASIL and control groups in topological properties and correlations between the properties and cognitive scores in the DMN. (A) Nodal efficiency and degree centrality were significantly different between the CADASIL and healthy control groups in the left DMN. The CADASIL had decreased nodal efficiency and degree centrality in the left dMPFC and HF. (B) Linear correlations between network properties in the DMN and cognitive scores in CADASIL. CADASIL, cerebral autosomal dominant arteriopathy with subcortical infarcts and leukoencephalopathy; DMN, default mode network; dMPFC, dorsal medial prefrontal cortex; HF, hippocampal formation; HC, healthy control; DG, degree centrality; NE, nodal efficiency; MoCA, Montreal Cognitive Assessment; MMSE, Mini-Mental State Examination.

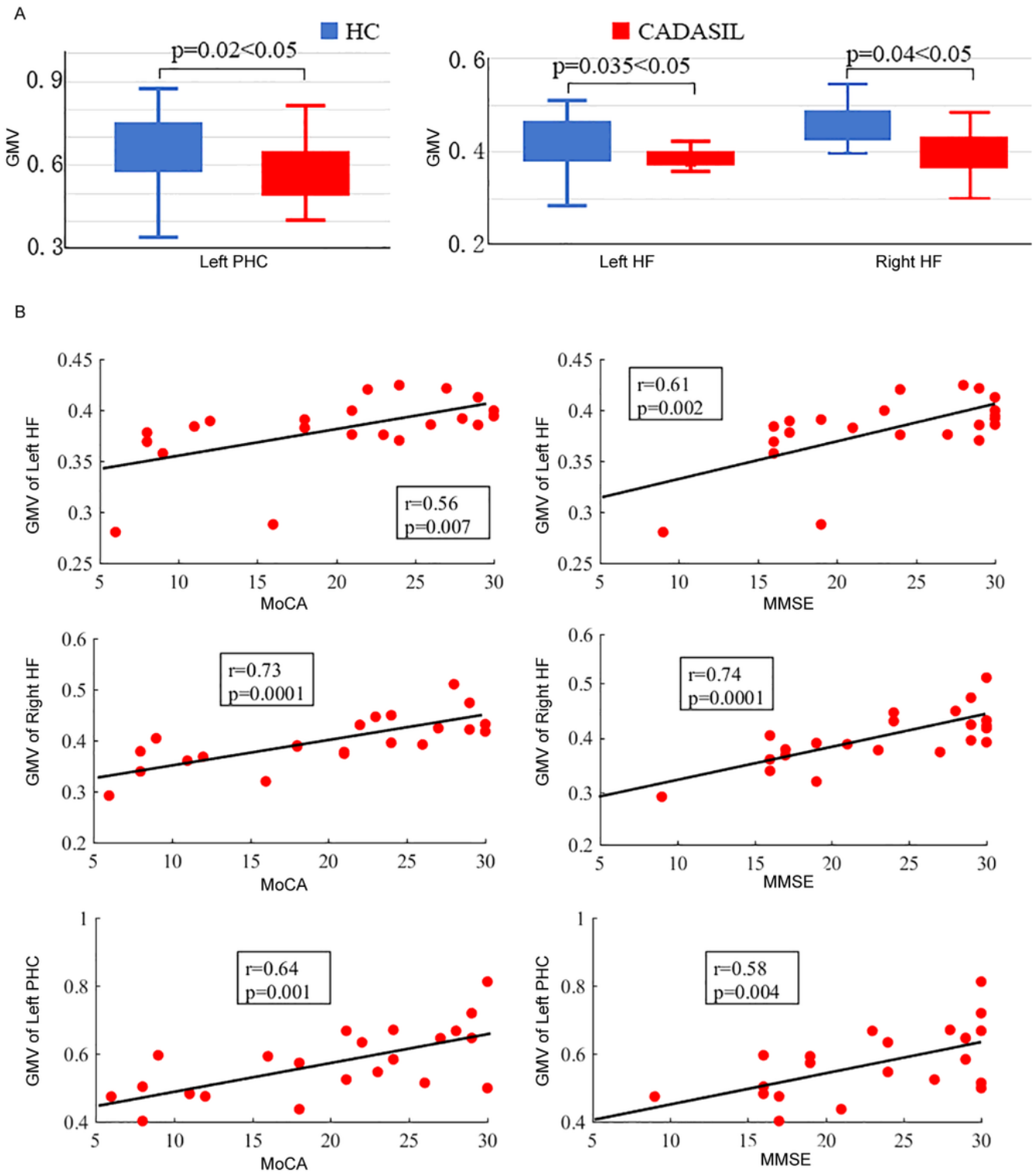

Figure 3

Results of GMV analysis in CADASIL and control groups. (A) Alterations in GMV of the DMN in CADASIL. CADASIL patients had decreased GMV in the left PHC and bilateral HF compared to healthy controls. (B) Correlations between GMV of ROIs within the DMN and cognitive scores in CADASIL. GMV, gray matter volume; CADASIL, cerebral autosomal dominant arteriopathy with subcortical infarcts and leukoencephalopathy; DMN, default mode network; PHC, parahippocampal cortex; HF, hippocampal

formation; ROI, region of interest; HC, healthy control; MoCA, Montreal Cognitive Assessment; MMSE, Mini-Mental State Examination.

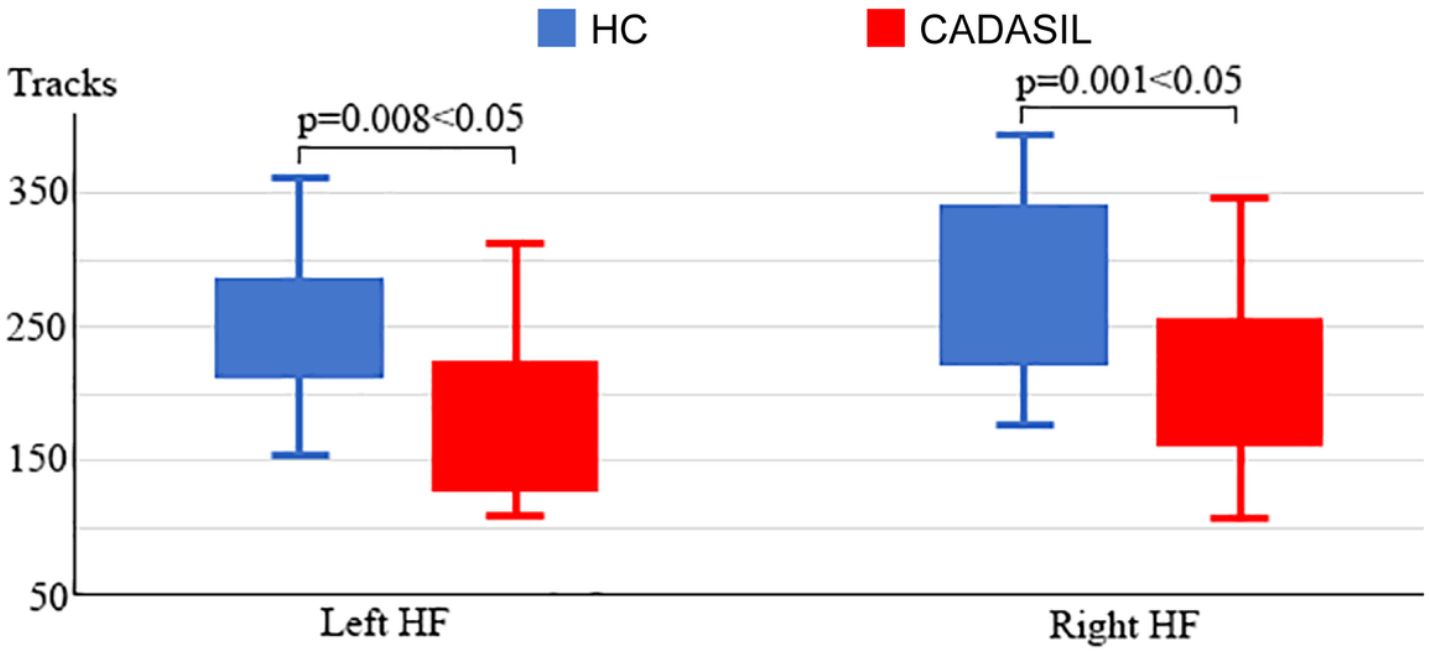

Figure 4

Analysis of fiber tracks in the DMN in CADASIL and control groups. CADASIL patients had decreased fiber tracks in the bilateral HF. DMN, default mode network; CADASIL, cerebral autosomal dominant arteriopathy with subcortical infarcts and leukoencephalopathy; HF, hippocampal formation; HC, healthy control.

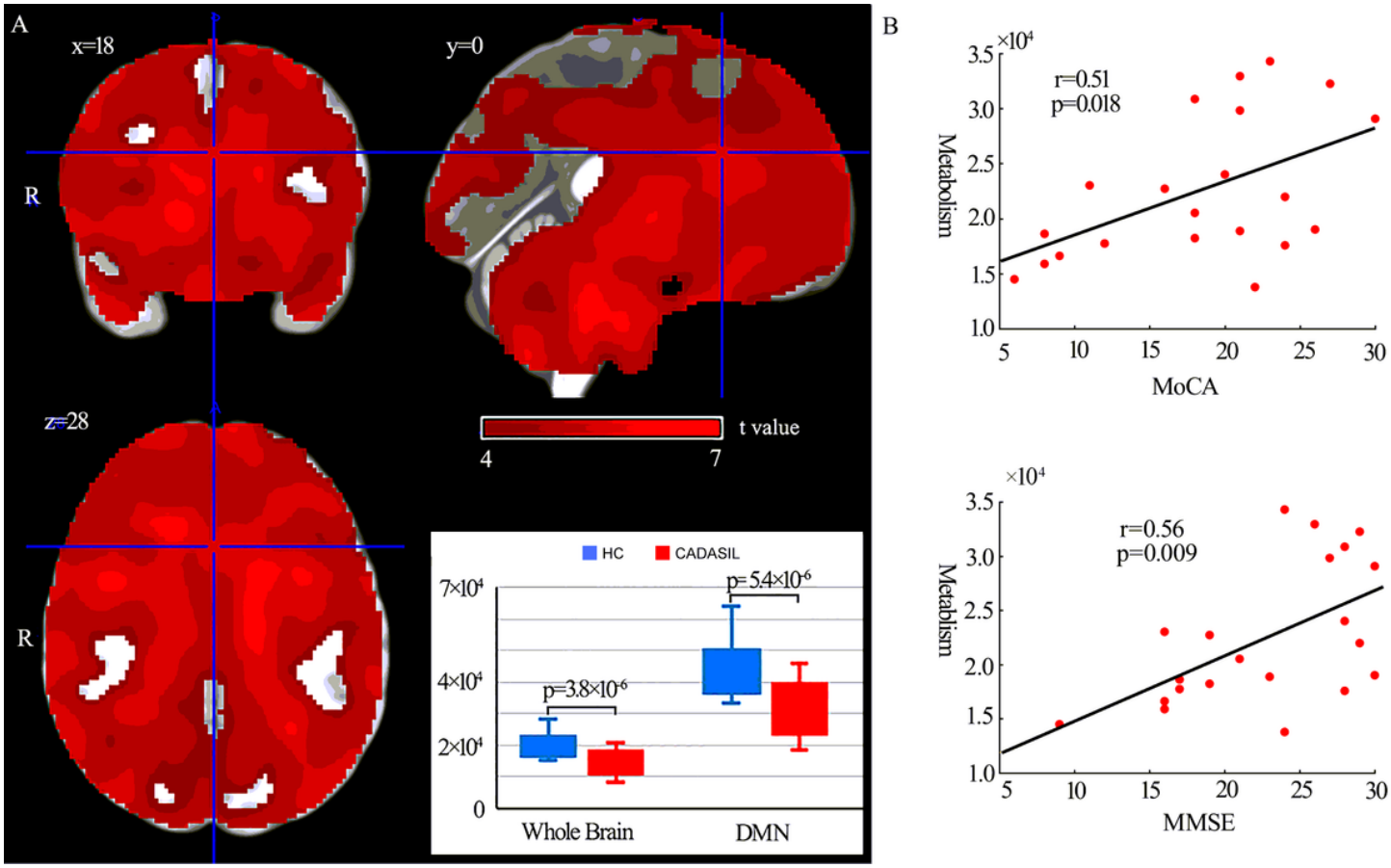

Figure 5

Results of metabolism analysis in the DMN in CADASIL and control groups. (A) Metabolism alterations in the CADASIL group. (B) Correlations between metabolism across ROIs within the DMN and cognitive scores in the CADASIL group. CADASIL patients had decreased metabolism across the whole brain, including the ROIs within the DMN, compared to healthy controls. DMN, default mode network; CADASIL, cerebral autosomal dominant arteriopathy with subcortical infarcts and leukoencephalopathy; ROI, region of interest; HC, healthy control; MoCA, Montreal Cognitive Assessment; MMSE, Mini-Mental State Examination.

Supplementary Files

This is a list of supplementary files associated with this preprint. Click to download.

- Additionalfile1.pdf